Ann Nucl Med (2014) 28:484–497
DOI 10.1007/s12149-014-0828-7

TECHNICAL NOTE

Performance evaluation of the eXplore speCZT preclinical imaging system

Ichiro Matsunari · Yoshiharu Miyazaki · Masato Kobayashi · Kodai Nishi · Asuka Mizutani · Keiichi Kawai · Akiko Hayashi · Ryoko Komatsu · Shoko Yonezawa · Seigo Kinuya

Received: 31 March 2013 / Accepted: 19 February 2014 / Published online: 8 March 2014

Abstract
Objective The eXplore speCZT is a recently introduced cadmium zinc telluride-based preclinical SPECT system that has a stationary detector design with interchangeable rotating collimators. Our aim was to evaluate the performance of the eXplore speCZT using ^{99m}Tc-sources. In particular, the image quality was assessed using the National Electrical Manufacturers Association NU-4 image quality phantom as well as an in vivo mouse.
Methods Energy resolution, sensitivity and spatial resolution were measured using ^{99m}Tc sources. Image quality was assessed using NU-4 image quality phantom. The measurements were performed for 4 available collimators: (1) mouse 7-pinhole collimator (mouse PH); (2) mouse 8-slit collimator (mouse SL); (3) rat 5-pinhole collimator (rat PH); and (4) rat 5-slit collimator (rat SL). Furthermore, a mouse bone imaging study was performed using mouse PH and mouse SL.
Results The system achieved the energy resolution of 5.5 % in full-width at half maximum (FWHM) at 140 keV using a ^{99m}Tc source. Without resolution recovery function, the system provided a near millimeter transaxial and axial spatial resolution using mouse PH. Mouse SL and rat SL provided reasonably good transaxial (1.79–2.00 mm in FWHM), but much worse axial resolutions (4.55–4.96 mm in FWHM). The use of resolution recovery significantly improved spatial resolution by in average 31 ± 3 or 35 ± 4 % in FWHM or full-width at tenth maximum, respectively. In particular, a sub-millimeter resolution of 0.71 mm in FWHM was achieved in either transaxial or axial direction with mouse PH. Using NU-4 phantom, the uniformity of slit collimators as expressed as percentage standard deviation was generally better than that of pinhole collimators. The use of resolution recovery substantially improved uniformity for all the collimators tested, but caused some overestimation in recovery coefficient. Reconstruction settings such as iteration or subset number significantly affected image quality measures. Finally, bone images of acceptable quality were obtained in in vivo mouse using mouse PH with resolution recovery.
Conclusions The overall performance shows that the eXplore speCZT system is suitable for preclinical imaging-based research using small-animals.

Keywords Preclinical · Cadmium zinc telluride · SPECT

I. Matsunari (✉) · Y. Miyazaki · A. Hayashi · R. Komatsu · S. Yonezawa
Clinical Research Department, The Medical and Pharmacological Research Center Foundation, Wo 32, Inoyama, Hakui, Ishikawa 925-0613, Japan
e-mail: matsunari@mprcf.or.jp

M. Kobayashi · K. Nishi · A. Mizutani · K. Kawai
School of Health Sciences, College of Medical, Pharmaceutical and Health Sciences, Kanazawa University, Kanazawa, Japan

S. Kinuya
Department of Nuclear Medicine, Kanazawa University Hospital, Kanazawa, Japan

Introduction

Preclinical molecular imaging such as SPECT and PET using small-animals is increasingly recognized as an important tool for biomedical research and new drug development [1–3]. In particular, SPECT equipped with multi-pinhole collimators enables small-animal imaging with high spatial resolution and reasonable sensitivity [1]. There are several such systems that are commercially available for current use [4–8], most of which use NaI-

based detectors. Alternatively, some newer detectors developed for small-animal SPECT incorporate semiconductor materials such as cadmium zinc telluride (CZT) [9], which directly convert gamma-rays to electric signal. As compared to conventional NaI-based detectors, CZT is attractive because it can be segmented to provide a high intrinsic spatial resolution [9]. Furthermore, high-energy resolution of CZT is beneficial for high contrast imaging by reducing scatter and multi-isotope imaging [1]. More importantly, the small size of CZT detectors enables compact designs [9], by which it is possible to surround the subject by an array of detectors. Such CZT-based cameras are now commercially available for clinical cardiac SPECT, resulting in improved image quality and shorter acquisition time [10–12].

The eXplore speCZT (GE Healthcare, Milwaukee, WI, USA) is a recently introduced commercially available preclinical SPECT system using a full ring 10 CZT-based detectors equipped with interchangeable collimators. It can be operated as a stand-alone SPECT system or can be combined with micro-CT. To date, however, there are no data available in literature that systematically assessed the imaging performance of the speCZT. More importantly, image quality of CZT-based small-animal SPECT has not been addressed in a standardized manner such as that using the National Electrical Manufacturers Association (NEMA) NU-4 image quality phantom [13].

The aim of this study was to evaluate the performance of CZT-based preclinical imaging system (eXplore speCZT) in view of energy resolution, sensitivity, spatial resolution, and image quality using ^{99m}Tc-sources. In particular, the image quality was assessed using NU-4 image quality phantom as well as an in vivo mouse.

Methods

System description

Features of the speCZT system are summarized in Table 1. This system has a stationary detector design with interchangeable rotating collimators. As illustrated in Fig. 1, the detector consists of 10 CZT-based detector panels surrounding the field of view (FOV). Each CZT detector panel consists of 32 × 32 arrays with the pixel size of 2.46 mm × 2.46 mm. There are 4 collimators provided by the manufacturer (Fig. 1): (1) mouse 7-pinhole collimator (mouse PH); (2) mouse 8-slit collimator (mouse SL); (3) rat 5-pinhole collimator (rat PH); and (4) rat 5-slit collimator (rat SL). The transaxial and axial FOVs vary depending on collimator geometry. The pinhole collimators are designed for high resolution images with small regions of interest, whereas slit collimators are designed for larger FOV (e.g., whole-body imaging) with reasonable spatial resolution [14, 15]. Although the axial FOVs of pinhole collimators are small, these can be set to a larger value (≤250 mm) in the helical acquisition mode with bed motion. The system saves each event of the acquired data in a list-mode format including its energy, and gated

Table 1 Features of the speCZT System

Detector configurations	
Material	Cadmium–zinc telluride
Detector length, width, and thickness (mm)	80, 80, 5
Type and number of detectors	Fixed-ring, 10
Number of arrays (size)	32 × 32 (2.46 mm)
Energy range	20–250 keV
Data collection	List-mode
ECG and respiratory gating capability	Yes
Collimator configurations	
Material	Tungsten
Mouse PH	
Number of pinholes	7
Diameter of pinhole (mm)	1
Single-bed position FOV diameter (mm)	32
Single-bed position FOV axial (mm)	25
Bore diameter (mm)	54
Radius of rotation/focal length (mm)	32.5/87.5
Rat PH	
Number of pinholes	5
Diameter of pinhole (mm)	1
Single-bed position FOV diameter (mm)	76
Single-bed position FOV axial (mm)	38
Bore diameter (mm)	89
Radius of rotation/focal length (mm)	50/70
Mouse SL	
Number of slits	8
Width of slit (mm)	1.23
Single-bed position FOV diameter (mm)	32
Single-bed position FOV axial (mm)	80
Bore diameter (mm)	64
Radius of rotation/focal length (mm)	37.5/82.5
Rat SL	
Number of slits	5
Width of slit (mm)	1.23
Single-bed position FOV diameter (mm)	76
Single-bed position FOV axial (mm)	80
Bore diameter (mm)	89
Radius of rotation/focal length (mm)	50/70

Mouse PH mouse 7-pinhole collimator, *Rat PH* rat 5-pinhole collimator, *Mouse SL* mouse 8-slit collimator, *Rat SL* rat 5-slit collimator, *FOV* field of view

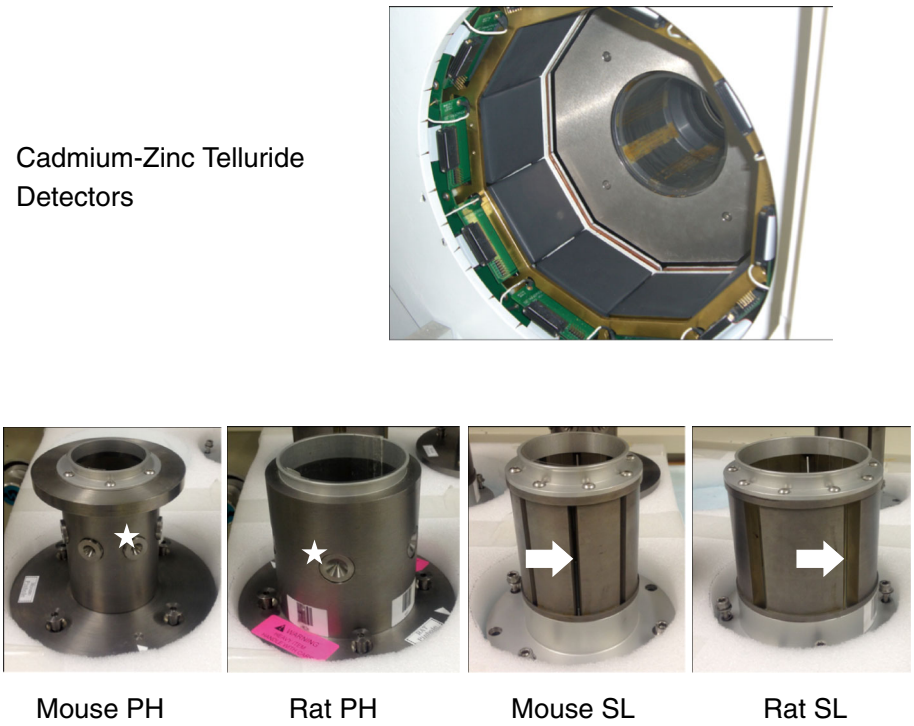

Fig. 1 Cadmium zinc telluride detectors built in the system (*upper*) and collimators (*lower*). Mouse PH indicates mouse 7-pinhole collimator; *Rat PH* rat 5-pinhole collimator, *Mouse SL* mouse 8-slit collimator; *Rat SL* rat 5-slit collimator. *Star* denotes pinhole; *arrow* slit

electrocardiogram (ECG)/respiratory motion trigger, for later specialized analysis. Images can be reconstructed by the three-dimensional maximum-likelihood expectation maximization (MLEM) or ordered subset expectation maximization (OSEM) method.

Energy resolution

Energy spectra within an energy window of 50–200 keV were obtained using a ^{99m}Tc point source, which was located in the center of FOV, and mouse PH. Energy resolution was measured based on the system as a whole, and was expressed as the full-width at half maximum (FWHM) as percentage of 140 keV energy peak, which was determined by direct measurement of histogram values.

Reconstruction settings

Unless specified, all the images were reconstructed using MLEM with 50 iterations with and without resolution recovery function. The number of iterations ($n = 50$) was tentatively determined in this study after testing several iteration numbers by visual inspection. The resolution recovery feature in this system was based on the modeling of pinholes and slits [16], including the modeling of geometrical structure, the material and related photon physics of the collimators. The energy window was set to 125–150 keV. Because the image matrix voxel size had to be varied according to collimator choice and imaging procedure, the voxel size used for each measurement was detailed in the following sections. No post-reconstruction filtering was applied. Neither attenuation nor scatter correction was performed.

To assess the effects of reconstruction settings on image quality measures, we tested the effects of iteration numbers ($n = 5$, 10, 20, 30, 40, 50, 60, 70, 80, 90, 100, and 200) for MLEM on image quality using NU-4 phantom. These measurements were made for all types of collimators. Images were reconstructed with and without resolution recovery function.

Sensitivity and spatial resolution measurements

System sensitivity was measured for each collimator with a ^{99m}Tc point source that was mounted on the imaging bed in the center of transaxial and axial FOVs. The activity of the point source was 3.5 MBq. The energy window was set to 125–150 keV. Projection data were acquired in step-and-shoot mode over 360° in 3° increment at 60 s/projection. The photon counts were obtained from projection images. System sensitivity was defined as the recorded counts per second divided by the decay-corrected activity of the point source.

Spatial resolution was measured for each collimator using a glass capillary line source. A glass capillary of inner diameter 0.14 mm (outer diameter 0.55 mm) was filled with 370 MBq/mL of ^{99m}Tc-solution and was placed in the center of the transaxial FOV and was aligned axially.

For axial resolution measurements, the glass capillary was placed horizontally in the center of the axial FOV. Projection data were acquired in step-and-shoot mode over 360° in 1.06° increment for mouse PH, which was the manufactural standard setting, or 1° for the other 3 collimators at 30 s/projection. The image matrix voxel sizes for transaxial spatial resolution measurements were 0.2 mm × 0.2 mm × 0.2 mm for mouse PH, 0.2 mm × 0.2 mm × 2.46 mm for mouse SL, 0.4 mm × 0.4 mm × 0.4 mm for rat PH, or 0.4 mm × 0.4 mm × 2.46 mm for rat SL, because reconstructed *z*-axis pixel size with slit collimators was always fixed to 2.46 mm, which was equal to the detector pixel size. For axial resolution measurements, we changed *z*-axis pixel size to 0.2 mm for mouse SL or 0.4 mm for rat SL using trilinear interpolation function in PMOD 2.7 (PMOD technologies Ltd., Zurich, Switzerland). Count profiles of the reconstructed transaxial images across the voxel having the maximum voxel intensity were plotted in the horizontal and vertical directions. The FWHM and full-width at tenth maximum (FWTM) were then determined by Gaussian fitting of the line profile. The averages of the horizontal and vertical directions were calculated over ten transaxial slices. FWHM and FWTM values of the axial profiles were obtained in the same way as the coronal images of the rotated source. The results of resolution measurements were not corrected for the source dimensions.

Image quality assessment

Image quality assessment was performed using the NU-4 image quality phantom [17], which had originally been developed for evaluating animal PET system and subsequently applied to animal SPECT system [5, 13]. The phantom has internal dimensions of 50-mm length and 30-mm diameter. The phantom consists of three compartments: a fillable uniform region, five fillable rods of different diameters (1, 2, 3, 4, and 5 mm) and two non-radioactive chambers filled with water or air (15-mm length; outer diameter of 10 mm; and wall thickness of 1 mm). The phantom was filled with 50 MBq of ^{99m}Tc solution and was scanned for 30 min using each collimator; 350 views from 7 pinholes (50 views/pinhole) at 36 s/view in 1.06 degree increment for mouse PH, 360 views from 8 slits (45 views/slit) at 40 s/view in 1 degree increment for mouse SL, 360 views from 5 pinholes (72 views/pinhole) 25 s/view in 1 degree increment for rat PH, and 360 views from 5 slits (72 views/slit) 25 s/view in 1° increment for rat SL. These acquisition settings were determined so that projection data cover over 360° with 1 or near 1° increment, and with comparable acquisition time among the collimators tested. For the mouse PH, where the axial FOV of 25 mm is smaller than the inner length (50 mm) of the NU-4 phantom, the acquisition was performed twice to cover the entire phantom. Images were reconstructed with the voxel size set to 0.5 mm × 0.5 mm × 0.5 mm for mouse PH or rat PH and 0.5 mm × 0.5 mm × 2.46 mm for mouse SL or rat SL. In addition, we performed acquisition of the NU-4 image quality phantom using mouse PH and helical scan mode. The acquisition parameters to cover the entire phantom were 165 steps at 11 s/step in 1° increment, resulting in a total acquisition time of 30 min. The image matrix voxel size was 0.33 mm × 0.33 mm × 0.33 mm. This was because the voxel size of helical SPECT using mouse PH was always fixed to 0.33 mm, which was automatically determined by table motion step size.

In this study, we performed the NU-4 phantom analyses based on NEMA recommendations for performance evaluation of small-animal PET [18]. A 22.5-mm diameter and 10-mm (or 2.46 mm × 4 mm for slit collimators) depth cylindrical volume of interest (VOI) was drawn over the center of the uniform region of the phantom. The percentage standard deviations (%STD) in the VOI were reported as a measure of uniformity. For mouse PH, where axial FOV was smaller than the length of phantom, %STDs from the 2 acquisitions, which covered the upper and lower portion of the uniform region (5-mm depth for each portion) were averaged. Spill-over ratios (SORwat and SORair) were calculated by drawing VOI's of diameter 4-mm and 7.5-mm (or 2.46 mm × 3 mm for slit collimators) length on the water- and air-filled cylindrical chambers. Then, the ratio of the mean counts in each cold region to the mean of the hot uniform area was reported as SOR.

To obtain the recovery coefficients (RC) for the filled rods, the reconstructed image slices covering the central 10-mm (or 2.46 mm × 4 mm for slit collimators) length of the rods were averaged to obtain a single slice. Circular regions of interest (ROIs) were drawn on this image, around each rod and background, with diameters twice the physical diameter of the rods. The background ROIs were placed outside the rod ROIs, where no activity was seen by visual inspection, and were processed in a manner that was used for the rod ROIs. The maximum values in each of these ROIs were measured on the averaged image. Then, the transverse image pixel coordinates of the locations with the maximum ROI values were transferred to the original unaveraged slices and were used to create line profiles along the rods in the axial direction. The mean and standard deviation of the pixel values measured along each rod or background line profile, based on the locations with maximum pixel value on the averaged image, were calculated. Then, the RC for the filled rods were obtained as the mean values in each rod line profile divided by the mean value obtained in the uniformity test described above

[17]. The standard deviation of the RC (STD_{RC}) was calculated as follows [18]:

$$STD_{RC} = SQRT\{(STD_{interprofile}/average_{interprofile})^2 + (STD_{background}/average_{background})^2\}. \quad (1)$$

In Eq. (1), SQRT denotes square root, $STD_{interprofile}$ and $average_{interprofile}$ are the standard deviation and average of a rod line profile, and $STD_{background}$ and $average_{background}$ are the standard deviation and average of background.

To assess the effects of reconstruction settings on RC, we newly introduced an index of error in RC using a formula as follows:

$$\text{Index of error in RC} = SQRT\{ (1 - RC_{rod1})^2 + (1 - RC_{rod2})^2 + (1 - RC_{rod3})^2 + (1 - RC_{rod4})^2 + (1 - RC_{rod5})^2. \quad (2)$$

In Eq. (2), SQRT denotes square root, RC_{rod1} is RC in 1-mm diameter rod, RC_{rod2} is RC in 2-mm diameter rod, RC_{rod3} is RC in 3-mm diameter rod, RC_{rod4} is RC in 4-mm diameter rod and RC_{rod5} is RC in 5-mm diameter rod.

The idea behind this index is that (1) in ideal situation, the RC is expected to be 1 irrespective of rod diameter; (2) therefore, the sum of absolute differences between ideal (RC = 1) and measured RC for each rod should provide an estimate of error in measured RC that reflects errors in all rods of NU-4 phantom. Such an index would be useful to determine optimal reconstruction parameters based on RC values.

Animal imaging

To assess the overall system performance, the imaging capabilities of the scanner were assessed through additional in vivo imaging studies. A normal mouse (SAMR1, 28.8 g, Nihon SLC Co, Ltd, Hamamatsu, Japan) was injected with 40 MBq of ^{99m}Tc-methylene diphosphonate (^{99m}Tc-MDP) via tail vein, and anesthetized with 1.0–2.0 % isoflurane. At 2 h after injection, the mouse was imaged for 32 min using the mouse PH. Immediately after the first scan, the second scan was performed for another 32 min using the mouse SL. For imaging with pinhole collimator, the helical scan mode was used to cover the body of mouse. The image matrix voxel size was 0.33 mm × 0.33 mm × 0.33 mm for mouse PH, or 0.33 mm × 0.33 mm × 2.46 mm for mouse SL. All experiments were performed with the approval of the institutional committee for animal research in compliance with the position of the American Heart Association on use of research animals.

Results

Energy resolution

As illustrated in Fig. 2, the system achieved the energy resolution of 5.5 % in FWHM at 140 keV using a ^{99m}Tc source.

Sensitivity and spatial resolution

The results of sensitivity and spatial resolution measurements are summarized in Table 2. The highest sensitivity was achieved with mouse SL, followed by mouse PH, rat SL, and rat PH. Without resolution recovery function during reconstruction, the system provided a near millimeter transaxial and axial spatial resolution using mouse PH. Mouse SL and rat SL provided reasonably good transaxial (1.79–2.00 mm in FWHM), but much worse axial resolutions (4.55–4.96 mm in FWHM). The use of resolution recovery significantly improved spatial resolution by in average 31 ± 3 or 35 ± 4 %

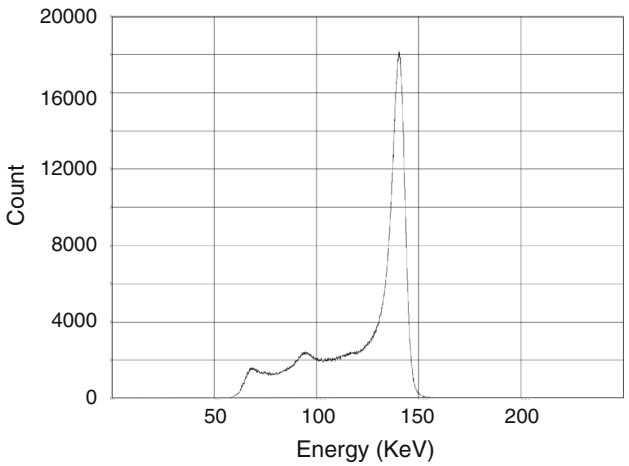

Fig. 2 Energy spectrum obtained from a ^{99m}Tc source

Table 2 Sensitivity and spatial resolution of the speCZT using each collimator

	Mouse PH	Rat PH	Mouse SL	Rat SL
Sensitivity (cps/MBq)	233.1	138.5	312.8	151.5
Spatial resolution in FWHM/FWTM (mm)				
Transaxial RR-on	0.71/1.28	1.20/2.18	1.26/2.29	1.47/2.68
Axial RR-on	0.71/1.30	1.11/2.02	3.13/5.70	3.14/5.72
Transaxial RR-off	1.11/2.02	1.81/3.29	1.79/3.27	2.00/3.64
Axial RR-off	1.04/1.90	1.83/3.35	4.55/8.30	4.96/9.03

FWHM full-width half maximum, *FWTM* full-width tenth maximum, *RR* resolution recovery filter

(average ± standard deviation) in FWHM or FWTM, respectively. In particular, a sub-millimeter resolution of 0.71 mm in FWHM was achieved in either transaxial or axial direction with mouse PH.

Image quality assessment using NU-4 phantom

The %STD of uniform region and SORs in the water and air compartments for each collimator are summarized in Table 3. The uniformity of slit collimators as expressed as %STD was generally better than that of pinhole collimators. The use of resolution recovery substantially improved uniformity in all collimators. The %STD values for the helical scan were higher than those for the single circular orbit scan using mouse PH. The SORs in water were slightly (2–30 %) higher than those in air for all collimators. The use of resolution recovery slightly lessened the SORs for each collimator. RCs and corresponding STD_{RC} as a function of rod diameter are shown in Fig. 3a, b, respectively. Without resolution recovery, the RC generally increased as a function of rod diameter, although it reached plateau at 4 mm with mouse PH or mouse SL. When resolution recovery function was used, the RC peaked at 2- to 3-mm rod diameter with values exceeding 1, and showed a subsequent decline. The $STDs_{RC}$ were generally larger with pinhole collimators than those with slit collimators. The use of resolution recovery lessened the STD_{RC} with pinhole collimators, but its effect was not significant with slit collimators. Both the RC and STD_{RC} for the helical scan were higher than those for the single circular orbit scan using mouse PH.

Transaxial NU-4 phantom images showing the uniform region along with line profiles, the region with water and air compartments, and the filled rods for each collimators with and without resolution recovery are shown in Fig. 4. By visual inspection, the images of uniform region were noisy with pinhole collimators, whereas those with slit collimators were more homogeneous. The images became more homogeneous with resolution recovery function. However, some edge enhancements were observed in the uniform region as well as the larger filled rods (3–5 mm) with resolution recovery, whereas such an edge enhancement was not seen without resolution recovery. Line profiles of uniform region essentially confirmed the observation described above.

Table 3 %STD of uniform region and spill-over ratios

	Mouse pinhole	Rat pinhole	Mouse slit	Rat slit
%STD RR-on (%)	19.3 (24.0)	10.3	6.0	8.1
%STD RR-off (%)	33.1 (50.6)	20.1	10.3	10.7
SOR-air RR-on	0.085 (0.073)	0.087	0.094	0.092
SOR-water RR-on	0.095 (0.095)	0.093	0.096	0.095
SOR-air RR-off	0.094 (0.090)	0.093	0.097	0.102
SOR-water RR-off	0.103 (0.108)	0.100	0.100	0.104

Data in parentheses are those by helical scan mode

Effects of reconstruction settings on image quality measures

Effects of iteration numbers for MLEM on the %STD of uniform region or SORs are illustrated for each collimator in Fig. 5a, b. The %STD increased as a function of iteration in all the collimators. The pinhole collimators showed more rapid increase in %STD as compared with the slit collimators. The use of resolution recovery function significantly lessened the %STD values in all the collimators, but did not have a major impact on SORs. The %STD values of <20 % were obtained with the iteration number of ≤100 with resolution recovery for rat PH; ≤200 for rat SL; ≤50 for mouse PH; or ≤200 for mouse SL. By contrast, the SORs in both water and air decreased as a function of iteration. With resolution recovery function, the SOR values of <0.1 in both water and air were obtained with the iteration number of ≥50 for any type of collimators tested in this study.

The RC values as a function of iteration numbers are illustrated in Fig. 6a, and indices of error in RC in Fig. 6b. The RC values rapidly increased as the iteration number increased, which was followed by gradual increase or decrease depending on rod diameter, collimator choice, and the use of resolution recovery function. The index of error in RC rapidly decreased as the iteration number increased, which was followed by gradual increase or decrease depending on collimator choice and the use of resolution recovery function. With resolution recovery function, the index of error in RC values of <1 was obtained with the iteration number of 30–100 for rat PH; ≥30 for rat SL; ≥10 for mouse PH; or ≥50 for mouse SL.

When the %STD of <20 %, the SOR of <0.1 in both water and air, and the index of error in RC of <1 were considered to be "good" image quality measures, these requirements were met with the iteration numbers of 50–100 for rat PH; 50–200 for rat SL; 50 for mouse PH; or 50–200 for mouse SL, when resolution recovery function was applied. Without resolution recovery function, these were met with 60–100 iterations for rat SL or 60–90 iterations for mouse SL, but were never met for rat PH or mouse PH.

In vivo bone images

Figure 7 shows 3D maximum intensity projection images of bone SPECT of a mouse acquired with mouse PH or mouse SL. Without resolution recovery, the image with

mouse PH was very noisy, which substantially improved after the use of resolution recovery. The image with mouse SL was less noisy, but detailed bone structures were not clearly seen because of lower axial resolution. The use of resolution recovery again improved image quality.

Discussion

To the best of our knowledge, this is the first study that has reported the imaging performance of speCZT system particularly using NU-4 image quality phantom. The major findings of this study were that (1) this system yielded a high-energy resolution of 5.5 % in FWHM; (2) a sub-millimeter resolution was achieved using mouse PH with reasonable sensitivity, but axial resolution was much worse with slit collimators; (3) the NU-4 image quality phantom results showed better uniformities with slit collimators as compared with pinhole collimators; (4) resolution recovery during reconstruction improved spatial resolution and uniformity, but caused some overestimation of recovery coefficient with NU-4 phantom; (5) reconstruction settings

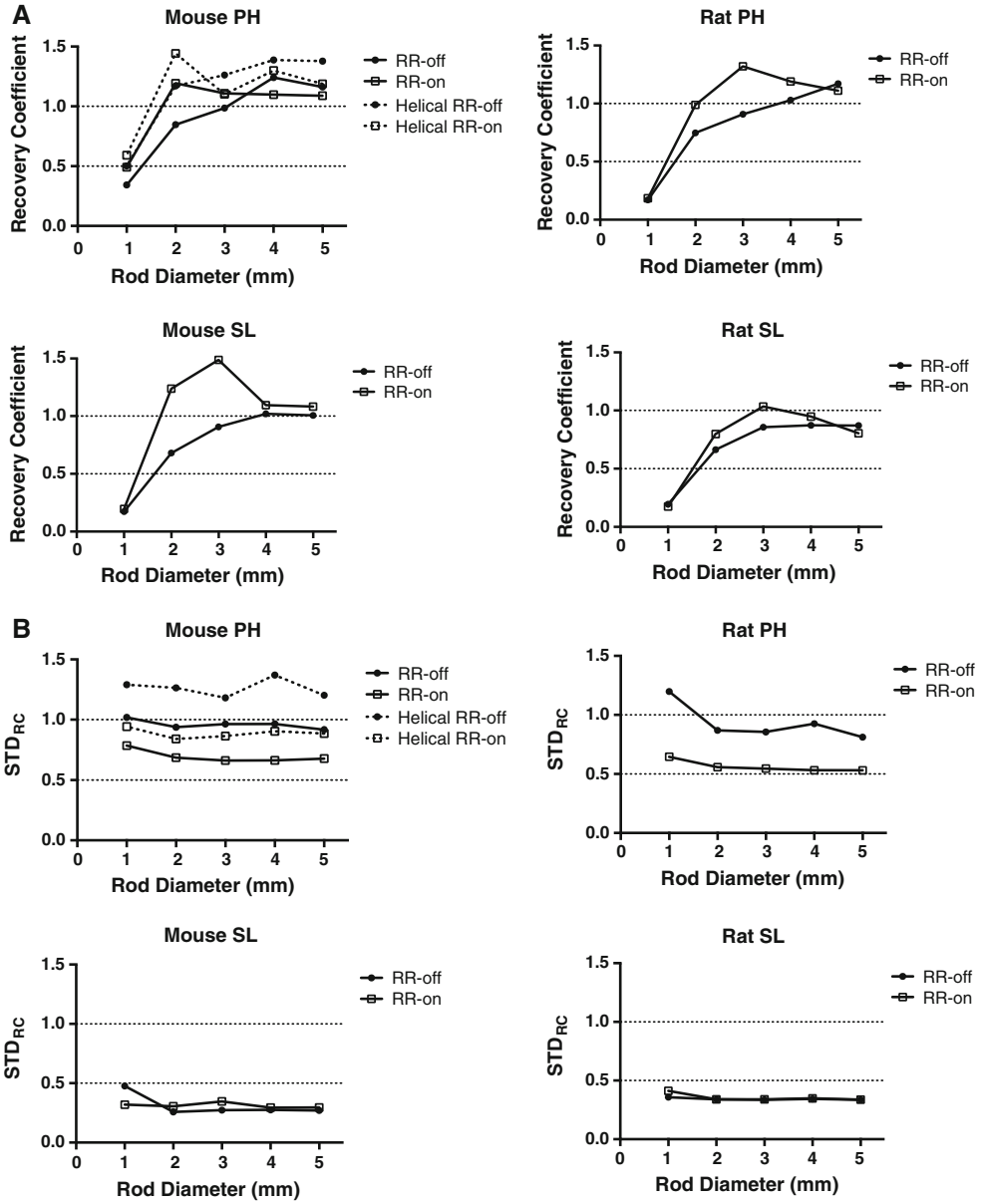

Fig. 3 Recovery coefficients (**a**) and STD_{RC} (**b**) for each collimator as a function of diameter of ^{99m}Tc-filled rods with and without resolution recovery. *Dot lines* denote values obtained by helical scan mode. *Mouse PH* mouse 7-pinhole collimator, *Rat PH* rat 5-pinhole collimator, *Mouse SL* mouse 8-slit collimator, *Rat SL* rat 5-slit collimator, *RR-on* with resolution recovery function, *RR-off* without resolution recovery

such as iteration number significantly affected image quality measures; and (6) bone images of acceptable quality were obtained in an in vivo mouse particularly using mouse PH with resolution recovery.

Energy resolution

A major advantage of CZT detector system is its high-energy resolution, which enables high contrast imaging by scatter rejection [10]. It should also be beneficial for simultaneously acquired multi-isotope imaging. Our results demonstrated that CZT detector system yielded a much higher energy resolution (5.5 % in FWHM) than those generally reported for NaI (12–15 %) [5, 19]. Furthermore, our result was comparable to that reported for a clinical CZT-based camera with essentially identical detector units (5.4 % in FWHM) [10].

Sensitivity and spatial resolution

In general, sensitivity is the measure of rate at which events are detected in the presence of radioactive sources, and depends on system configuration such as aperture size, the number of apertures, radius of rotation and detector material. As mentioned earlier, this system has 10 CZT-based detectors with 5–7 pinhole or slit collimators with 1.0-mm diameter or slit width and 32.5- to 50-mm radius of rotation. The results showed that the sensitivity was in order of a couple of hundred cps/MBq, and varied depending on collimator choice. The sensitivity achieved in this study was lower than those reported for U-SPECT II [8] that has 3 stationary NaI detectors equipped with a collimator having a total of 75 pinholes with 0.35- to 1.0-mm diameter, but higher than that reported for Inveon SPECT [5] that has 2 NaI detectors with single pinhole collimators with 0.5- to 1.0-mm diameter (a total of 2 pinholes) or first generation CZT-based SPECT [9] that has 8 detectors with single pinhole collimators with 0.5-mm diameter (a total of 8 pinholes), and comparable to that reported for another CZT-based small-animal SPECT system (FX3200, Gamma-Medica Ideas, CA, USA) [20] that has 4 detectors with single- or 5-pinhole collimators with 0.5-mm diameter (a total of 5 or 20 pinholes). Thus, our results on sensitivity seem to be reasonable for the commercially available animal SPECT cameras.

The spatial resolution is primarily determined by collimator aperture, detector size, magnification, and intrinsic detector resolution. Despite the much smaller detector size and thereby smaller magnification as compared to NaI-based detectors [5, 8], the mouse PH achieved spatial resolution comparable to those reported for other commercially available small-animal SPECT systems [5], which is due to the small detector pixel size (2.46 mm) of detector. This is particularly true when resolution recovery during reconstruction was applied, which improved spatial resolution by approximately 30 %. Slit collimator apertures provide an opportunity for larger axial FOV imaging as compared to pinhole apertures [1, 15]. However, the disadvantage of slit collimator is a loss of axial resolution because there is no axial magnification. Therefore, slit collimators (mouse SL and rat SL) provided reasonable transaxial, but much worse axial resolution in this study.

Fig. 4 **a** Transaxial images of NU-4 image quality phantom acquired using 4 collimators reconstructed with (RR-on; *right*) and without (RR-off; *left*) resolution recovery. Images are normalized to the peak activity on each image. **b** Line profile across the uniform region. *Mouse PH* mouse 7-pinhole collimator, *Rat PH* rat 5-pinhole collimator, *Mouse SL* mouse 8-slit collimator, *Rat SL* rat 5-slit collimator, *RR-on* with resolution recovery function, *RR-off* without resolution recovery

Image quality assessment using NU-4 phantom

To date, no standardized method exists for assessing imaging performance of small-animal SPECT. Therefore, we used NU-4 phantom that had originally been developed to assess small-animal PET [17], which has also turned out to be useful for SPECT [13]. Our results showed that the uniformity as assessed by %STD was better with slit collimators than pinhole collimators. This is to some extent because of the longer axial voxel size of slit collimators (2.46 mm) as compared with that of pinhole collimators (0.5 mm), which was unavoidable due to system configuration. Furthermore, the uniformity was significantly improved for all the collimators by the use of resolution recovery function. This is explained by the noise reduction feature by resolution recovery [11, 21]. At present, it is difficult to determine whether %STD values obtained in this study are acceptable for practical use because there is no established threshold value available for this purpose. However, the %STD values using U-SPECT-II (MILabs, Utrecht, the Netherlands) and NU-4 phantom with radioactivity equal to that in our study (50 MBq) ranged from approximately 8–30 % without post-reconstruction filtering [13]. Other SPECT systems have also reported %STD values of 9.2–20.5 % [5, 20], which are comparable to those with resolution recovery observed in this study. Thus, the sensitivity uniformity as expressed by %STD in our system seems to fall within the expected range.

The SORs largely reflect photon scatter from outside the cold chamber as well as that originating in the cold chamber itself. Therefore, the higher SORs-water than SORs-air observed in this study is likely to be caused by the stronger scatter in water than that in air. However, the difference in SORs between water and air (2–12 %) seems to be somewhat smaller than those reported for NaI-based

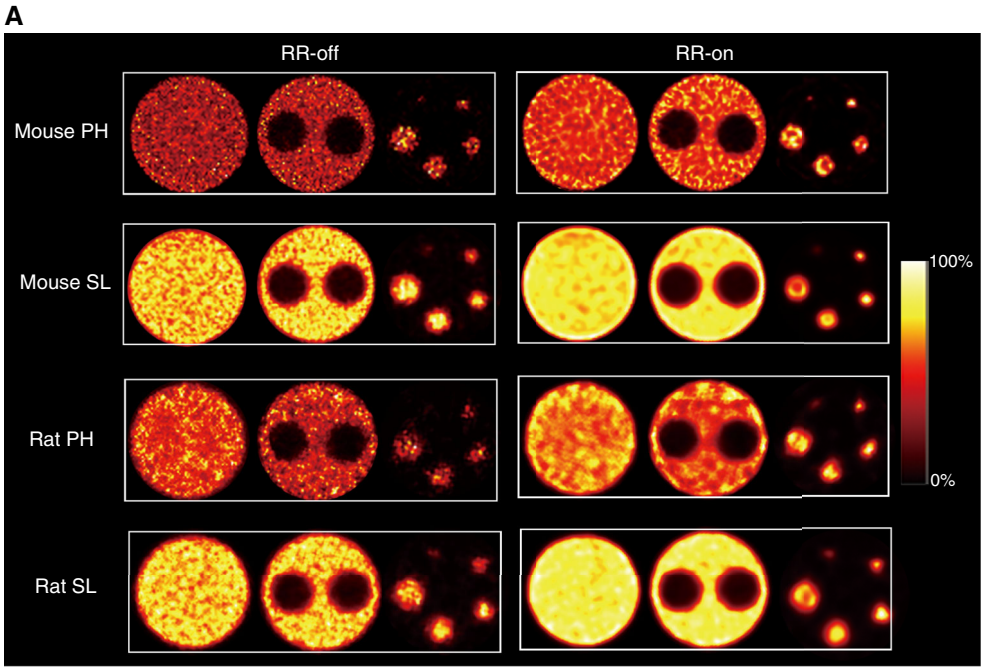
A
RR-off
RR-on
Mouse PH
Mouse SL
Rat PH
Rat SL
100%
0%

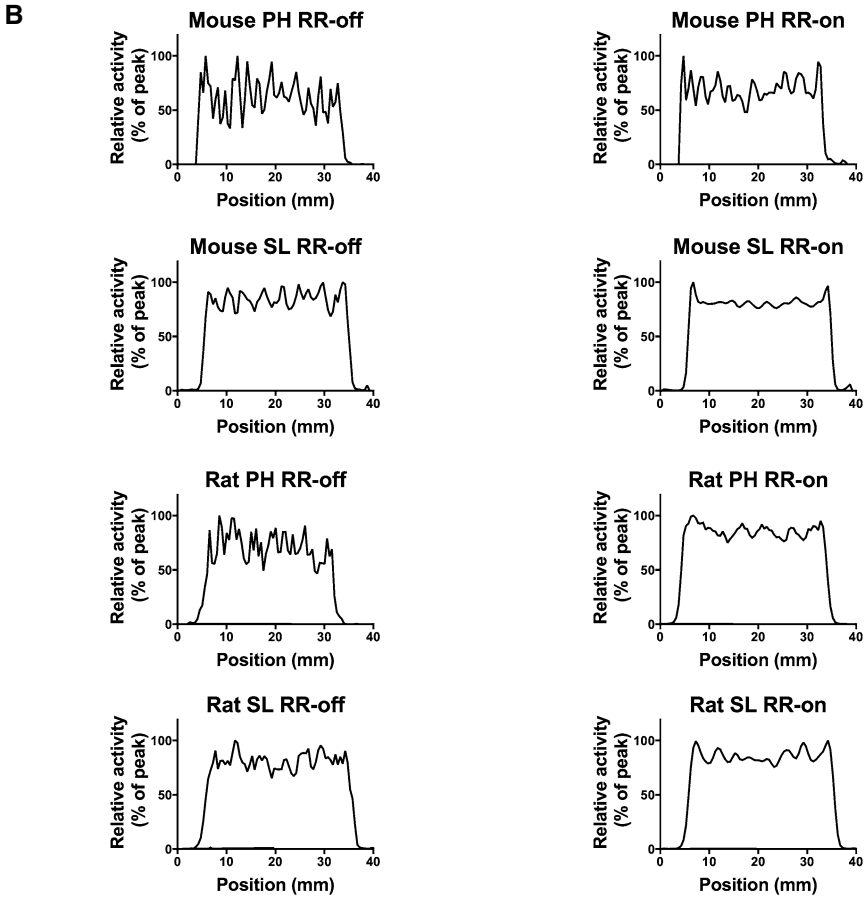
B
Mouse PH RR-off
Mouse PH RR-on
Mouse SL RR-off
Mouse SL RR-on
Rat PH RR-off
Rat PH RR-on
Rat SL RR-off
Rat SL RR-on
Relative activity (% of peak)
Position (mm)
0
50
100
0
10
20
30
40

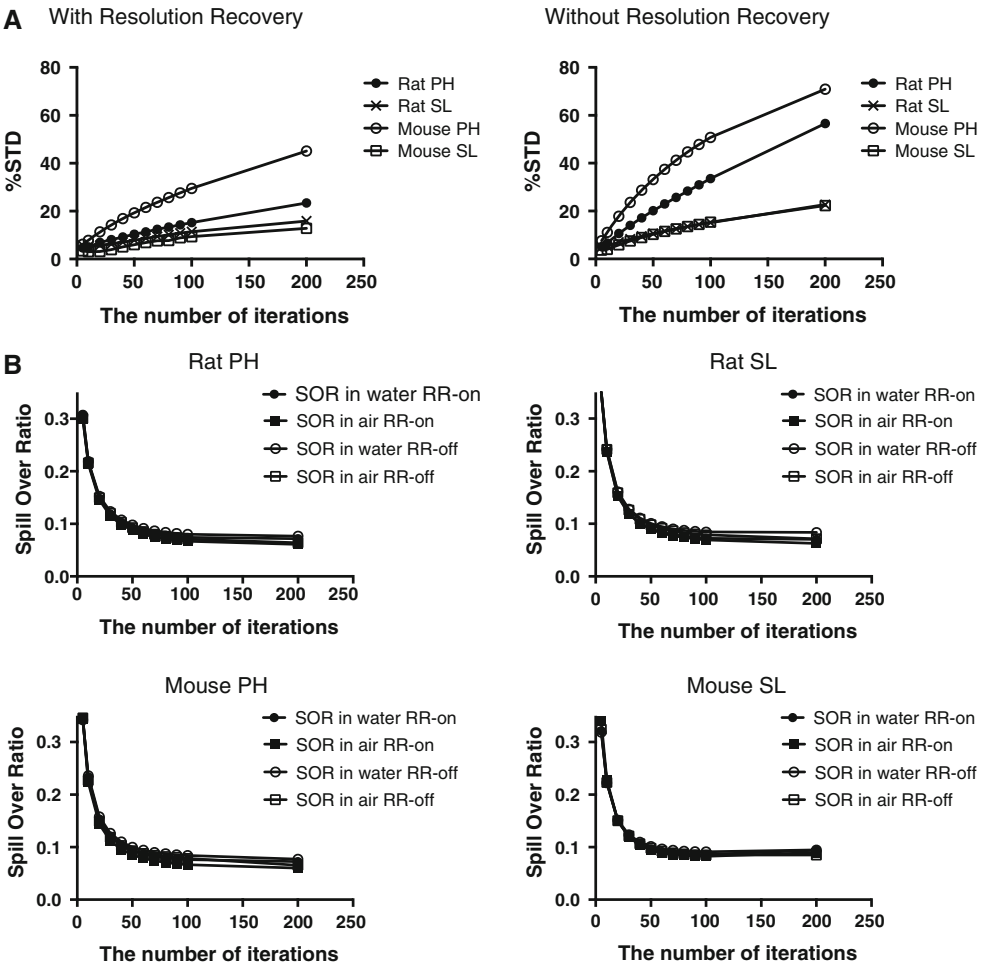

Fig. 5 **a** The %STD of uniform region of NU-4 image quality phantom as a function of iteration numbers for maximum-likelihood expectation maximization (MLEM) plotted for each collimator with and without resolution recovery function during reconstruction. **b** Spill-over ratios as a function of iteration numbers for MLEM plotted for each collimator with and without resolution recovery function. *Mouse PH* mouse 7-pinhole collimator, *Rat PH* rat 5-pinhole collimator, *Mouse SL* mouse 8-slit collimator, *Rat SL* rat 5-slit collimator, *RR-on* with resolution recovery function, *RR-off* without resolution recovery, *SOR* spill-over ratios

SPECT [13]. This may reflect differences in system configuration (CZT versus NaI) and reconstruction setting between the studies. As demonstrated in this study, CZT detector has a much higher energy resolution than NaI-based detector, resulting in less scatter fraction. Furthermore, it is known that reconstruction settings such as the number of iteration affect SORs as demonstrated in this study and others [13]. These mechanisms may have contributed to our results. It is notable that the use of resolution recovery lessened both SOR-water and SOR-air. Although the precise mechanisms are not clear, this may also be related to improvement of partial volume effect by resolution recovery. The RC serves as a surrogate measure of spatial resolution that could be compared with other imaging systems [13]. Our results showed that RC generally increased as a function of rod diameter without resolution recovery, but it exceeded 1 at 2- to 3-mm rod diameter with resolution recovery, indicating that the resolution recovery function causes overestimation of activity in some circumstances. This is likely to be because of overestimation of activity due to edge enhancement. In 2- to 3-mm diameter rods, such edge enhanced regions could be overlapped, resulting in significant overestimation of activity. The edge enhancement phenomena with resolution recovery were also notable in uniform region of NU-4 phantom images as well as its line profiles.

The $STDs_{RC}$, which are recommended to measure in NEMA NU-4 standards [18], were obtained as an index of stability in RC that would reflect image noise. Our results showed that the $STDs_{RC}$ were larger for pinhole collimators than those for slit collimators, and that the use of resolution recovery significantly lessened STD_{RC} values particularly for pinhole collimators. These trends are similar to those observed for %STD of uniform region.

Pinhole versus slit collimator

In vivo imaging is important for overall assessment of image quality. The bone images of a mouse demonstrated that acceptable image quality can be obtained with a 40 MBq of the administered tracer activity and reasonably acceptable acquisition time (32 min) if resolution recovery function is turned on. As expected from the results of phantom studies, detailed structure was not visible with

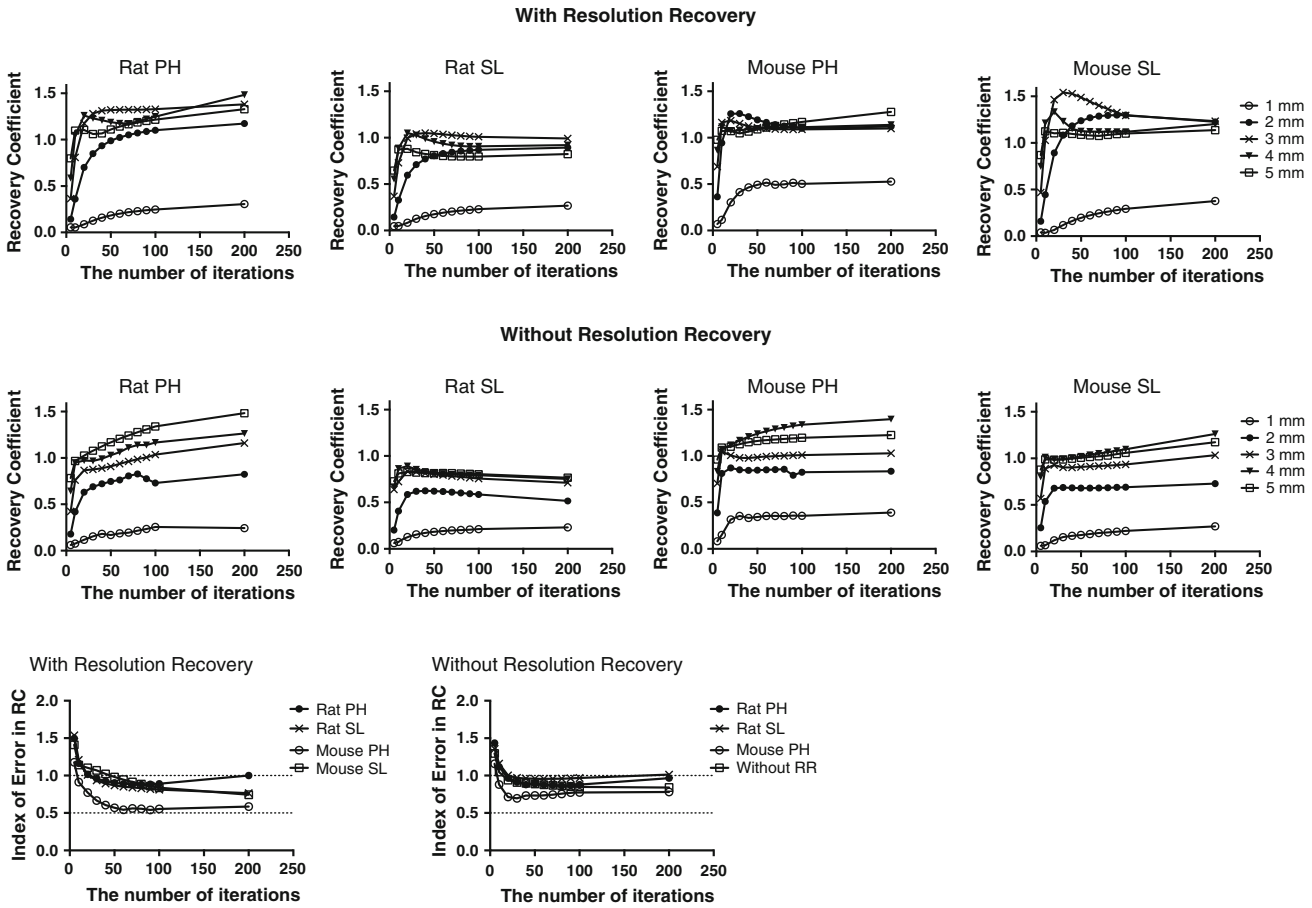

Fig. 6 **a** Recovery coefficients (RC) of NU-4 image quality phantom as a function of iteration numbers for maximum-likelihood expectation maximization (MLEM) plotted for each collimator with (*upper*) and without (*lower*) resolution recovery function during reconstruction. **b** Index of error in RC as a function of iteration numbers for MLEM plotted for each collimator with (*upper*) and without (*lower*) resolution recovery function. *Mouse PH* mouse 7-pinhole collimator; *Rat PH* rat 5-pinhole collimator, *Mouse SL* mouse 8-slit collimator, *Rat SL* rat 5-slit collimator

mouse SL because of much lower axial resolution than mouse PH. Based on these results, we would recommend to use mouse PH rather than mouse SL together with resolution recovery in this setting. In this study, we used the helical scan mode for in vivo imaging with mouse PH. A drawback of helical scan is, however, that it usually requires a large number of projections to scan entire mouse or rat body, because acquisition step angle and bed motion per step are fixed to 1.0° and 0.33 mm for mouse PH or 0.67° and 0.5 mm for rat PH in this system. For this reason, the helical scan with mouse PH presented in Fig. 4 required 242 scan steps as compared to 45 steps with mouse SL. Furthermore, the number of steps with the slit collimator can easily be reduced to, for example, 10 (increment angle of 4.5°). These indicate that a single scan time would be much shorter with slit collimator for a given acquisition time per step. When the acquisition time per step is set to the minimal (i.e., 1 s), for example, a single scan with mouse SL would require only 10 s as compared to 242 s with mouse PH. As such, slit collimators should be useful for dynamic imaging of an entire mouse or rat body, where multiple serial short acquisitions are required. However, the value of slit collimator for dynamic imaging needs to be addressed in further studies, because we focused on comparative evaluation of imaging performance with comparable acquisition time among the collimators.

Effect of resolution recovery

We applied resolution recovery function during reconstruction based on the modeling of pinholes and slits [16] in this study, reflecting recent advances in iterative reconstruction algorithms. The results showed that the use of resolution recovery improves spatial resolution, uniformity, SOR, and overall image quality. This is in line with the published results in that the resolution recovery during reconstruction generally provides improved resolution and lower noise magnitude in the images [11, 21]. Therefore, in

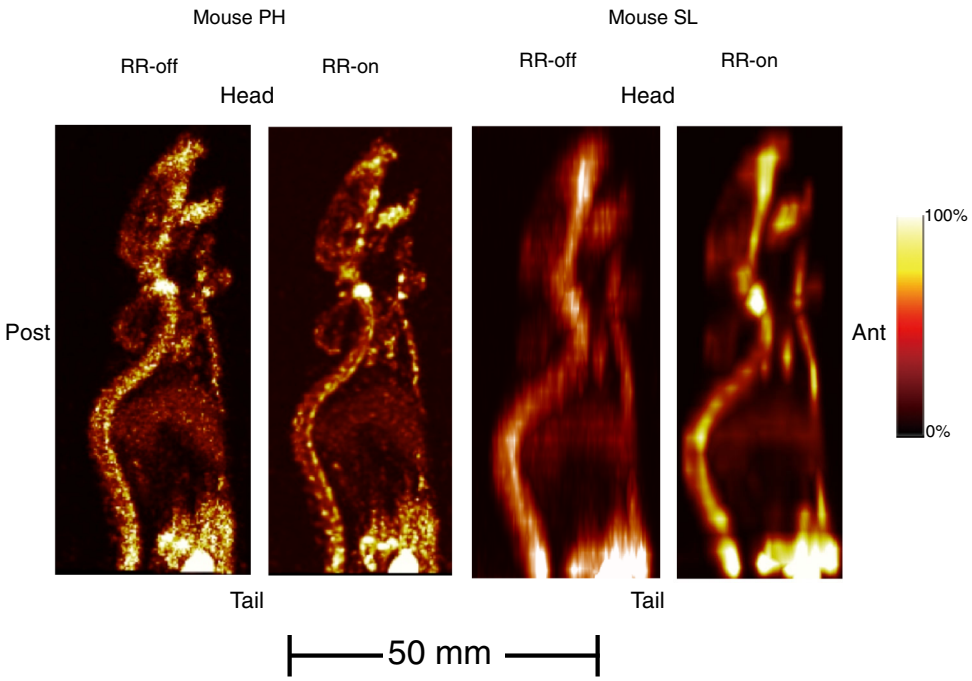

Fig. 7 3D maximum intensity projection images of a mouse bone SPECT using either mouse PH (*left*) or mouse SL (*right*) with (RR-on) and without resolution recovery (RR-off). *Mouse PH* mouse 7-pinhole collimator, *Mouse SL* mouse 8-slit collimator, *RR-on* with resolution recovery function, *RR-off* without resolution recovery

practical settings, it is preferable to use resolution recovery whenever possible as described earlier. However, our results also indicate that images reconstructed with resolution recovery should be interpreted with caution in that the pixel values may not necessarily guarantee quantitative accuracy as discussed earlier related to RC in NU-4 phantom. Therefore, a care should be taken when measuring activity of small objects with diameter of 2–3 mm, or object edge. In such cases, one could probably use images without resolution recovery function as an option.

Helical scan

In this study, we preferred to use a single circular orbit rather than a helical scan. This was because the helical scan in our system was less flexible in terms of voxel size and acquisition parameters such as step angle per view. For example, the voxel size was always fixed to 0.33 mm × 0.33 mm × 0.33 mm and step angle was set to 1 degree for mouse PH with no other options available. However, a helical scan has an advantage over a single circular orbit scan in that it can cover long axial FOV. Furthermore, a single circular orbit scan with pinholes for a long object may cause axial blurring and may affect analysis for performance evaluation. Therefore, we performed a helical scan of the NU-4 image quality phantom using mouse PH in addition to the more conventional single circular orbit scan. We observed higher %STD values of the uniform region with the helical scan than those with the single circular orbit scan. This was likely because of smaller voxel size for the helical scan (0.33 mm × 0.33 mm × 0.33 mm) than that for the single circular orbit scan (0.5 mm × 0.5 mm × 0.5 mm). Moreover, imaging of the entire phantom using two 30-min scans of single circular orbit (a total of 60 min) was longer than that using helical scan (30 min). These circumstances in the helical scan may have caused a high noise level and thereby a high %STD. We also observed higher RC and STD_{RC} values with the helical scan. The smaller voxel size for the helical scan may have caused less partial volume effects than those for the single circular orbit scan, resulting in the higher RCs. The higher STD_{RC} values for the helical scan were likely to be explained by the higher noise due to the smaller voxel size and shorter acquisition time because, as mentioned earlier, the STD_{RC} would reflect image noise. In practice, we would recommend to use a single circular orbit scan when the target object is small such as heart or brain, because it is more flexible in terms of voxel size and acquisition parameters. On the other hand, a helical scan would be useful in the circumstances where whole-body imaging is required, although more validations are necessary to optimize the imaging parameters.

Effects of reconstruction settings on image quality measures

The results showed that the %STD of sensitivity uniformity increased, while SORs decreased, as a function of iteration, which is in line with a study by Harteveld et al. [13]. Furthermore, the index of error in RC rapidly decreased as the iteration number increased, which was followed by gradual increase or decrease depending on collimator choice and the use of resolution recovery function. From a

practical point of view, an optimal reconstruction setting is one that provides relatively low %STD (e.g., <20 %), low SORs (e.g., <0.1), and low index of error in RC (e.g., <1). Our results showed that the suitable range of iteration numbers for MLEM reconstruction to meet such requirements is different depending on collimator choice. For example, the suitable range of iteration numbers with resolution recovery function was considered to be 50–100 for rat PH or 50 for mouse PH, whereas it was wider (50–200) for rat SL or mouse SL. Without resolution recovery function, it was considered to be 60–100 for rat SL or mouse SL. However, it was difficult to meet such requirements for pinhole collimators mainly due to higher %STDs. When higher %STDs (e.g., <40 %) were accepted, the suitable range of iteration numbers was considered to be 50–100 for rat PH or 50–60 for mouse PH. Thus, reconstruction settings should be optimized for each collimator with/without resolution recovery function.

Limitations

There are limitations of the study to be mentioned. First, although NU-4 phantom is successfully applied in small-animal PET scanners [17], it has not yet been optimized for animal SPECT with small FOV, which is necessary to achieve high spatial resolution and sensitivity. For example, NU-4 phantom cannot be used for very small radius of rotation. Conversely, the phantom with larger diameter would be better for the collimators for rat imaging. These are the limitations of NU-4 phantom for evaluating small-animal SPECT, where system design becomes more diverse in recent years. Second, we focused on ^{99m}Tc as a radionuclide to be tested in this study, because it is widely used and many of imaging performance test results are reported based on it [5, 8, 9, 13], which provides an opportunity for comparison of systems. Other radionuclides such as ^{123}I or ^{111}In, which are also used for molecular imaging, should be tested in future.

Conclusions

The performance of the eXplore speCZT system has been characterized for each collimator using phantoms including the NEMA NU-4 image quality phantom and an in vivo mouse. The results indicate that the scanner has a high-energy resolution and reasonable sensitivity and spatial resolution. The image quality phantom results indicate that the use of resolution recovery function significantly improves the spatial resolution as well as image quality, although images with resolution recovery should be interpreted with caution in that the pixel values may not necessarily guarantee quantitative accuracy. The overall performance shows that the eXplore speCZT system is suitable for preclinical imaging-based research using small-animals.

Acknowledgments This work was supported by Ishikawa prefectural government.

Conflict of interest None of the authors have conflicts to disclose.

References

1. Franc BL, Acton PD, Mari C, Hasegawa BH. Small-animal SPECT and SPECT/CT: important tools for preclinical investigation. J Nucl Med. 2008;49:1651–63.
2. de Kemp RA, Epstein FH, Catana C, Tsui BM, Ritman EL. Small-animal molecular imaging methods. J Nucl Med. 2010;51(Suppl 1):18S–32S.
3. Bravo PE, Bengel FM. The role of cardiac PET in translating basic science into the clinical arena. J Cardiovasc Transl Res. 2011;4:425–36.
4. Beekman FJ, van der Have F, Vastenhouw B, van der Linden AJ, van Rijk PP, Burbach JP, et al. U-SPECT-I: a novel system for submillimeter-resolution tomography with radiolabeled molecules in mice. J Nucl Med. 2005;46:1194–200.
5. Magota K, Kubo N, Kuge Y, Nishijima K, Zhao S, Tamaki N. Performance characterization of the Inveon preclinical small-animal PET/SPECT/CT system for multimodality imaging. Eur J Nucl Med Mol Imaging. 2011;38:742–52.
6. Metzler SD, Jaszczak RJ, Patil NH, Vemulapalli S, Akabani G, Chin BB. Molecular imaging of small animals with a triple-head SPECT system using pinhole collimation. IEEE Trans Med Imaging. 2005;24:853–62.
7. Umeda IO, Tani K, Tsuda K, Kobayashi M, Ogata M, Kimura S, et al. High resolution SPECT imaging for visualization of intratumoral heterogeneity using a SPECT/CT scanner dedicated for small animal imaging. Ann Nucl Med. 2012;26:67–76.
8. van der Have F, Vastenhouw B, Ramakers RM, Branderhorst W, Krah JO, Ji C, et al. U-SPECT-II: an ultra-high-resolution device for molecular small-animal imaging. J Nucl Med. 2009;50:599–605.
9. Kim H, Furenlid LR, Crawford MJ, Wilson DW, Barber HB, Peterson TE, et al. SemiSPECT: a small-animal single-photon emission computed tomography (SPECT) imager based on eight cadmium zinc telluride (CZT) detector arrays. Med Phys. 2006;33:465–74.
10. Bocher M, Blevis IM, Tsukerman L, Shrem Y, Kovalski G, Volokh L. A fast cardiac gamma camera with dynamic SPECT capabilities: design, system validation and future potential. Eur J Nucl Med Mol Imaging. 2010;37:1887–902.
11. Garcia EV, Faber TL, Esteves FP. Cardiac dedicated ultrafast SPECT cameras: new designs and clinical implications. J Nucl Med. 2011;52:210–7.
12. Gimelli A, Bottai M, Giorgetti A, Genovesi D, Kusch A, Ripoli A, et al. Comparison between ultrafast and standard single-photon emission CT in patients with coronary artery disease: a pilot study. Circ Cardiovasc Imaging. 2011;4:51–8.
13. Harteveld AA, Meeuwis AP, Disselhorst JA, Slump CH, Oyen WJ, Boerman OC, et al. Using the NEMA NU 4 PET image quality phantom in multipinhole small-animal SPECT. J Nucl Med. 2011;52:1646–53.
14. Walrand S, Jamar F, de Jong M, Pauwels S. Evaluation of novel whole-body high-resolution rodent SPECT (Linoview) based on direct acquisition of linogram projections. J Nucl Med. 2005;46:1872–80.

15. Zheng GL, Gagnon D. CdZnTe strip detector SPECT imaging with a slit collimator. Phys Med Biol. 2004;49:2257–71.
16. Bal G, Acton PD. Analytical derivation of the point spread function for pinhole collimators. Phys Med Biol. 2006;51:4923–50.
17. Bao Q, Newport D, Chen M, Stout DB, Chatziioannou AF. Performance evaluation of the inveon dedicated PET preclinical tomograph based on the NEMA NU-4 standards. J Nucl Med. 2009;50:401–8.
18. NEMA Standards Publication NU 4-2008: Performance measurements of small animal positron emission tomographs. Rosslyn: National Electrical Manufacturers Association; 2008.
19. Zeniya T, Watabe H, Aoi T, Kim KM, Teramoto N, Takeno T, et al. Use of a compact pixelated gamma camera for small animal pinhole SPECT imaging. Ann Nucl Med. 2006;20:409–16.
20. Higaki Y, Kobayashi M, Uehara T, Hanaoka H, Arano Y, Kawai K. Appropriate collimators in a small animal SPECT scanner with CZT detector. Ann Nucl Med. 2013;27:271–8.
21. Vanhove C, Andreyev A, Defrise M, Nuyts J, Bossuyt A. Resolution recovery in pinhole SPECT based on multi-ray projections: a phantom study. Eur J Nucl Med Mol Imaging. 2007;34:170–80.